Recent progress in fluctuation theorems and free energy recovery

A. Alemany, M. Ribezzi-Crivellari, F. Ritort

Abstract

We review applications of fluctuation theorems to recover free energy differences from single molecule pulling experiments. The possibility of measuring energies in the range of tenths of kcal/mol or $k_{\mathrm{B}}T$ of molecular systems embedded in an aqueous environment opens exciting perspectives to our basic understanding of energy processes in nonequilibrium small systems. After a brief reminder of key concepts about free energy measurements and calculations we overview single-molecule manipulation techniques and free energy recovery using fluctuation theorems. Issues concerning the correct definition of mechanical work, the non-Galilean invariance of fluctuation theorems and free energy recovery from unidirectional work measurements are also discussed.

Contents

1 Introduction

Free energy is a key quantity in thermodynamics that combines the effects of two opposite trends in nature: the minimization of energy led by deterministic or ordering forces and the maximization of entropy induced by the randomness or noise of the environment. Free energy minimization determines the spontaneous evolution and final equilibrium state attained by thermal systems. The knowledge of free energy differences between different states of a system provides a deep insight of its response to external perturbations. This applies to systems ranging from single molecules to the entire universe.

One classical approach to free energy measurements is to quasi-statically (i. e. infinitely slow) change a control parameter and measure the net amount of energy exchanged between the system and the environment. The ultimate goal of these measurements is the determination of the free energy branches, which describe the dependence of the free energy of the system with the control parameter. At macroscopic scales the experimental outcomes of thermodynamic manipulations, be it quasi-static or not, do not significantly change over different repetition of the same protocol (meaning same system, source, initial state and process). Yet, this is true only for large enough systems. The situation is very different at microscopic scales, where outcomes from repetitions of an identical experimental protocol can be different. The origin of these fluctuations are thermal random forces caused by the environment that deliver uncontrolled amounts of energy to the system as the transformation is carried out.

Recent theoretical developments in nonequilibrium physics have shown how, using these fluctuations, it is possible to recover free energy differences and free energy landscapes from irreversible work measurements in thermodynamic transformations of small systems. These developments go under the name of fluctuation theorems and are reviewed in detail in other chapters of this book. From an experimental point of view, these theoretical results provide a powerful method to obtain thermodynamic quantities from experiments carried out in nonequilibrium conditions. In this chapter we will succinctly review some of the main developments in this field in the context of single molecule experiments and explain how fluctuation theorems can be applied to the measurement of free energies of folding in molecular structures. A few topics reviewed in this chapter have been already discussed in a previous paper by us [1].

The plan of this chapter is as follows: Section 2 contains a brief description of equilibrium-based bulk and computational methods to recover free energy differences. Section 3 describes the main experimental techniques used to manipulate small systems with special emphasis on DNA stretching experiments with optical tweezers. Section 4 overviews fluctuation relations and their usefulness to recover free energy differences from irreversible work measurements. Section 5 discusses issues related to the correct definition of control parameters, configurational variables and mechanical work in small systems. The right definition of mechanical work has generated some debate and confusion during the past years and we found this volume a good opportunity to clarify this point. In Section 6 we analyze an important extension of the Crooks fluctuation relation to the case where states are in partial (rather than global) equilibrium. Such extension allows for a full recovery of free energy branches and partially equilibrated states. Finally, we discuss the main limitations of free energy recovery when dissipation is too large and free energy estimates obtained from bidirectional and unidirectional methods too biased. The paper ends with some conclusions.

2 Free Energy Measurement prior to Fluctuation Theorems

The understanding of many biophysical processes does often require the knowledge of the underlying Free Energy (FE) differences. For instance, this is the case in the study of the folding behavior of proteins and nucleic acids, or ligand binding by proteins. Given the interest of these phenomena, several methods were developed to reliably measure FE changes in experiments or to estimate them through the combination of statistical mechanics and computational techniques. Before discussing the recently introduced non–equilibrium methods based on Fluctuation Relations we review the classical experimental and computational approaches to FE recovery.

2.1 Experimental Methods for FE measurements

Equilibrium thermodynamics offers several equalities between FE differences and directly measurable quantities: the most famous of these equalities links the FE difference between two equilibrium states (A and B) to the reversible work $W_{\rm rev}^{A\to B}$ needed to bring the system from state A to state B through a series of equilibrium states:

$$\Delta G_{AB} = W_{\rm rev}^{A\to B}, \tag{1}$$

where G is the Gibbs Free Energy, as we have in mind a situation in which temperature T and pressure P are controlled. A second important relation, suitable for the study of FE changes in chemical reactions, relates the FE difference between reagents (R) and products (P) to the equilibrium constant K of a reaction [2]:

$$\Delta G_{RP} = -N_A k_{\rm B} T \log K = -N_A k_{\rm B} T \log \frac{[P]}{[R]}, \tag{2}$$

where by $[\cdot]$ we denote molar concentrations, N_A is the Avogadro number (6.02×10^{23} mol^{-1}) and $k_{\rm B}$ is the Boltzmann constant (1.38×10^{-23} J/K). It is important to stress that these equations pertain to the domain of equilibrium thermodynamics and the validity of any result obtained through them is to be questioned whenever the assumption of thermodynamic equilibrium is violated.

The denaturation transition in proteins and nucleic acids (DNA, RNA) can be used to illustrate some of the equilibrium FE measurement methods. Denaturation, i.e. the loss of the native folded configuration, in proteins and nucleic acids can be induced by different means. Prominent examples are thermal and chemical denaturation. In thermal denaturation experiments unfolding is induced raising the temperature of the solution in which the molecules are stored. In chemical denaturation experiments, the unfolding is instead obtained raising the concentration of a denaturant (e.g. urea or guanidine), which interferes with the non–covalent interactions (hydrogen–bonds, Van der Waals forces) that stabilize the native configuration. The FE difference between the native and the unfolded state can be estimated by measuring the fraction of unfolded molecules as a function of the temperature or denaturant concentration and using Eq. (2). Several techniques are available to measure these populations; we will only cite some of the most common:

- **UV absorbance spectroscopy** uses the sample's absorbance at 287 nm as a probe of the relative population of the folded and unfolded state. This is possible because some amino-acid residues change their absorbance according to the surrounding environment. The optical density of Trypsin, for example, is decreased when it passes from an hydrophobic

environment (e.g. inside a folded protein) to an hydrophilic environment (e.g. exposed to a polar solvent).

- **Circular Dichroism (CD) spectroscopy** compares the differences in absorption of left-handed versus right-handed circularly polarized light. The double helix of nucleic acids and the different types of secondary structure in proteins (α–helix, β-sheet and random coil) have specific CD signatures in the far–UV region. From the CD spectrum of a sample it is possible to estimate how the fraction of each of these structures changes at different denaturation conditions [12].

- **Fluorescence spectroscopy** uses the natural fluorescence of Tryptophan, an amino-acid residue. Tryptophan is excited by a monochromatic light source with $\simeq$ 290 nm wavelength and the resulting fluorescence spectrum is analyzed through a monochromator (e.g. diffraction grating). Both the yield of Tryptophan fluorescence and the peak of the spectrum are sensitive to the environment. A Tryptophan buried in the hydrophobic core of a folded protein has a high yield and gives intense fluorescence, while in an hydrophilic environment it gives lower intensity. The fraction of folded proteins contained in a sample can be estimated measuring its fluorescence intensity.

Another common method for FE measurements is calorimetry. Most calorimetric methods rest on the thermodynamic equality relating FE to the specific heat at constant pressure, c_P:

$$\left(\frac{\partial^2 G}{\partial T^2}\right)_P = -\frac{c_P}{T}, \tag{3}$$

which allows FE recovery via the Gibbs-Helmholtz equation.

- **Differential Scanning Calorimetry (DSC)** is one of the most usual calorimetric techniques. DSC determines the constant pressure heat capacity (c_P) of a protein or nucleic acid in solution as function of the temperature [39]. The heat capacity is obtained as the ratio between the heat flux towards the sample and the temperature increase in the sample. Unfolding of the solute (protein or nucleic acids) induces a peak in the heat capacity, which is due to the extra heat needed to disrupt the non-covalent interactions which stabilize the native structure. The enthalpy or FE changes across the transition are measured by integration of the c_P.

FE recovery from both thermal and chemical denaturation experiments are based on a series of assumptions. These include matters such as the order of the denaturation transition, the reversibility of the denaturation process and the number of states in the transition region [45]. Moreover, the interpretation of denaturation experiments requires the formulation of a model for the effect of the denaturant on the FE, an issue which is often dealt with by a linear extrapolation. Nevertheless it is the need for reversibility which puts fundamental limits on the applicability of these classical techniques. For example in the last years many kinetically stable proteins, i.e. proteins whose native is not thermodynamically but just kinetically stable, have been discovered [39]. The stability of these proteins is difficult to be investigated by the aforementioned techniques.

2.2 Computational FE estimates

The combination of statistical mechanics and the continuously growing computational power have paved the way for numerical techniques to estimate FE changes. We will only review two classical approaches of Free Energy Calculations that are a limit case of the more general

techniques based on fluctuation relations: Thermodynamic Integration (TI, [23]) and the Free Energy Perturbation method (FEP, [50]).

Let us consider a system of N particles contained in a three–dimensional box at temperature T. The Hamiltonian of this system will be denoted by H_λ, where λ is a control parameter which distinguishes different states of the system (e.g. charge or dipole moment of the particles). The Helmholtz FE, ($F(N,V,T)$), which is the natural thermodynamic potential when temperature (T) and volume (V) are controlled, is linked to the canonical partition function $Z_\lambda(N,V,T)$ by:

$$F_\lambda(N,V,T) = -k_B T \ln Z_\lambda(N,V,T), \tag{4}$$

$$Z_\lambda(N,V,T) = \int \exp\left(-\frac{H_\lambda}{k_\mathrm{B}T}\right) d^{3N}x d^{3N}p. \tag{5}$$

The FE difference ΔF between two states of a system characterized by two different values of the control parameter λ (λ_A, λ_B) is, according to Eq. (4):

$$\Delta F = -k_B T \ln \frac{Z_{\lambda_B}}{Z_{\lambda_A}}. \tag{6}$$

Using the definition of partition function introduced in Eq. (5), Eq. (6) can be transformed as follows:

$$\begin{aligned}
\Delta F &= -k_\mathrm{B}T \log \frac{\int \exp\left(-\frac{H_{\lambda_B}}{k_\mathrm{B}T}\right) d^{3N}x d^{3N}p}{\int \exp\left(-\frac{H_{\lambda_A}}{k_\mathrm{B}T}\right) d^{3N}x d^{3N}p} = \\
&= -k_\mathrm{B}T \log \frac{\int \exp\left(-\frac{H_{\lambda_B}-H_{\lambda_A}}{k_\mathrm{B}T}\right) \exp\left(-\frac{H_{\lambda_A}}{k_\mathrm{B}T}\right) d^{3N}x d^{3N}p}{\int \exp\left(-\frac{H_{\lambda_A}}{k_\mathrm{B}T}\right) d^{3N}x d^{3N}p} = \\
&= -k_\mathrm{B}T \log \left\langle \exp\left(-\frac{H_{\lambda_B} - H_{\lambda_A}}{k_\mathrm{B}T}\right) \right\rangle_A
\end{aligned} \tag{7}$$

The FE difference between two states can thus be obtained averaging the exponential of the Hamiltonian difference, with respect to the Boltzmann distribution corresponding to one state. This could be done with Monte Carlo simulations. The use of Eq. (7) is limited by a practical problem: if the Hamiltonians defining the two states are very different, then also the "typical" configurations for the two states will be very different. As a consequence, the convergence of a numerical calculation can be impractically slow. One possible solution is to use the TI method, which uses a slightly modified version of Eq. (7). Taking the derivative of F_λ with respect to λ we get:

$$\frac{dF}{d\lambda} = \frac{\int \partial_\lambda H_\lambda \exp\left(-\frac{H_\lambda}{k_\mathrm{B}T}\right) d^{3N}x d^{3N}p}{\int \exp\left(-\frac{H_\lambda}{k_\mathrm{B}T}\right) d^{3N}x d^{3N}p} = \langle \partial_\lambda H_\lambda \rangle_\lambda, \tag{8}$$

so that the calculation of the FE difference between two states characterized by very different values of λ can be reduced to a series of smaller steps. The interested reader will find rich information on Free Energy Calculations, from the initial stages to the recent developments in [5].

3 Single molecule experiments

The boost experienced by nanotechnologies from 1990 to the present day have made it possible to manipulate a single molecule at a time by exerting forces in the range of piconewtons and measure molecular distances with nanometric resolution.

In traditional bulk experiments, like calorimetry or UV absorbance, samples under study contain a large number N of molecules. Experimental measurements are the result of an average over the behavior of all the molecules. Fluctuations are of the order of $1/\sqrt{N}$ and become negligible. In contrast, single molecule systems provide a powerful example of the so-called *small systems*, where fluctuations play an important role as they are of the same order of magnitude as the energy exchanged by the system with the environment [4, 36].

Small systems are not restricted to single molecules. On the one hand, fluctuations in the measurement of energy exchanges with the surroundings of any macroscopic system operating at short enough timescales could play an important role. On the other hand, if measurements in a molecular system are carried out over long times (compared to the heat diffusion time of the system) fluctuations become small and irrelevant. In this chapter we will focus our attention on single molecule experiments, a canonical example of small system manipulation.

3.1 Experimental techniques

There are several techniques that allow the manipulation of a single molecule at a time. Mostly used are the atomic force microscopy (AFM), magnetic tweezers (MT) and laser optical tweezers (OT). Differences between the three techniques appear when considering the operating range in force and distance and the choice of the control parameter to carry out experiments (see Section 5).

- The **AFM** is based on the principle that a cantilever with a tip can sense the roughness of the surface and deflect by an amount which is proportional to the proximity of the tip to the surface [17, 47]. The typical experimental setup in force spectroscopy experiments is as follows: a surface is coated with the desired molecules and the AFM tip is coated with molecules that can bind (either specifically or non-specifically) to the molecules on the substrate. By moving the tip to the substrate a contact between the tip and one of the molecules adsorbed on the substrate is made. Retraction of the tip at constant speed allows to measure the deflection of the cantilever in real time, providing (when its stiffness in known) the force acting on the molecule as a function of its end-to-end distance. The main drawback in AFM experiments is the presence of undesired interactions or the interaction of many molecules between the tip and the substrate. Different strategies, like the design of polyproteins, have been specifically developed to overcome these limitations.

  The AFM covers forces between 20-1000 pN depending on the stiffness of the cantilever. Typical values of the stiffness are in the range 10-1000 pN/nm. Resolution in the AFM is limited by thermal fluctuations. When the cantilever stage is held at a constant position the force acting on the tip and the extension between tip and substrate fluctuate. The respective r.m.s.d. are given by $\sqrt{\langle \delta x^2 \rangle} = \sqrt{k_{\mathrm{B}}T/k} \sim 2$ Å and $\sqrt{\langle \delta f^2 \rangle} = \sqrt{k_{\mathrm{B}}Tk} \sim 10$ pN where k_{B} is the Boltzmann constant, T is the absolute temperature of the environment and k is the stiffness of the cantilever, taken equal to 100 pN/nm. AFMs are ideal to investigate strong intermolecular and intramolecular interactions, e.g. pulling experiments in biopolymers such as polysaccharides, proteins and nucleic acids [10].

- **MT** are based on the principle that a magnetized bead with dipole moment μ experiences a force f when immersed in a magnetic field gradient B equal to $f = \mu \nabla B$. The typical experimental setup is as follows: a bead is trapped in the magnetic field gradient generated by two strong magnets and a molecule is attached between the surface of the magnetic bead and a glass surface. Molecules are pulled or twisted by moving the translation stage that supports the magnets. A microscope objective with a CCD camera is used to determine

the position of the bead, equal to the extension of the molecule x. Force is measured by using the expression $f = k_{\mathrm{B}}Tx/\langle \delta x^2 \rangle$ [46, 11].

Typical values of the magnetic trap stiffness are 10^{-4} pN/nm, which induces large fluctuations in the extension of the molecule, on the order of 20 nm. The typical range of operating forces is 10^{-2}-10 pN, where the maximum value of the force depends on the size of the magnetic bead. When the magnet stage is kept fixed the force acting on the bead can be kept constant because the spatial region occupied by the bead is small enough for the magnetic field gradient to be considered uniform. Therefore, although the bead position fluctuates the force is always constant. MT have been extensively used to investigate elastic and torsional properties of DNA molecules and processes involving molecular motors [28].

- The principle of **OT** is based on the optical gradient force generated by a focused beam of light acting on an object with an index of refraction higher than that of the surrounding medium [35, 27]. The typical experimental setup is as follows: a micron-sized polystyrene or silica bead is captured in the optical trap, while another bead is immobilized by air suction in the tip of a micropipette. Molecular biology tools are employed to insert a molecule between molecular handles, and the whole molecular complex is inserted between the two beads (see Fig. 1b). In a more recent setup, dual traps are also used.

  The operating force range in OT is (0.5-100) pN, depending on the size of the bead (on the order of 1-3 μm) and the power of the laser (few hundred milliwatts). To a very good approximation the trapping potential is harmonic, $f = kx$, where k is the stiffness constant of the trap and x is the distance of the trapped bead to the center of the optical trap. Typical values of the stiffness of the optical trap are 10^{-2}-10^{-4} times smaller than for AFM tips, therefore force resolution is at least 10 times better, on the order of 0.1 pN. Depending on the experimental set-up the spatial resolution can reach the nanometer level only in carefully isolated environments (absence of air currents, mechanical and acoustic vibrations and temperature oscillations). OTs have been widely used to investigate nucleic acids and molecular motors.

3.2 Pulling DNA hairpins with optical tweezers

Nucleic acids stretched under force are excellent model systems to explore the non-equilibrium physics of small systems. DNA hairpins are one of the most simple and versatile molecular systems one can think about. They consist of a stable DNA double helix, called stem, ended by a loop (Fig. 1a). When force is applied to both ends of the stem by pulling them apart, the basepairs establishing the stem become progressively disrupted until the DNA hairpin unfolds completely, around 15 pN (depending on the salt concentration, the temperature and the pulling speed).

The force range accessible with an optical tweezers instrument makes it an appropriate tool to study the behavior of DNA and RNA hairpins under mechanical force. In a pulling experiment with optical tweezers the two ends of a DNA hairpin are linked to double stranded DNA handles [44, 9]. One handle is attached to a polystyrene bead that is immobilized by air suction in the tip of a micropipette, whereas the other handle is attached to another polystyrene bead that is captured in the optical trap (Fig. 1b). Handles are used to avoid spurious interactions between the beads and the molecule under study. The relative distance λ between the center of the trap and the tip of the micropipette is the control parameter in these experiments. At the beginning of an unzipping experiment, both λ and the force applied to the system are low and the hairpin is in its folded conformation. Then λ is increased at a constant pulling speed until a maximum force is achieved, typically around 30 pN, where the hairpin is unfolded. In a rezipping experiment we

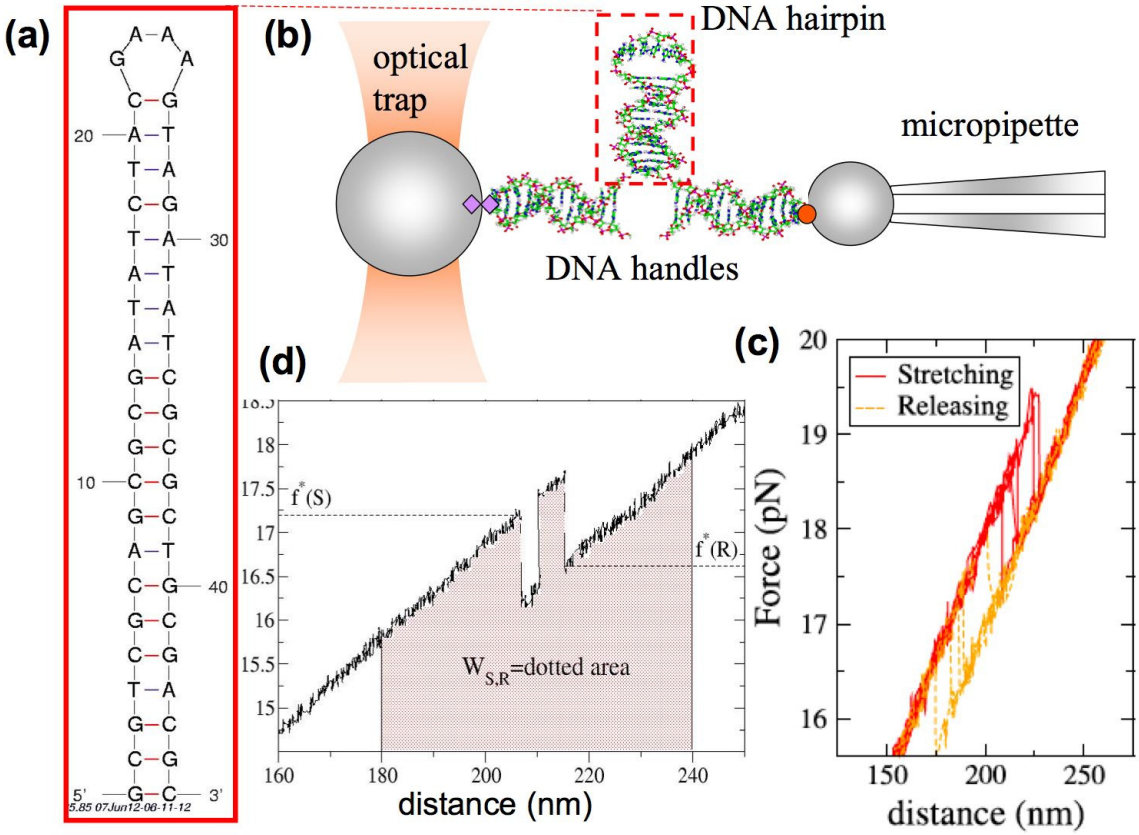

Figure 1: **Mechanical folding/unfolding of DNA hairpins.**(a) The sequence of a DNA hairpin with a 21bp stem ending in a tetraloop. Figure not to scale. (b) Experimental setup. A molecular construct made of the hairpin shown in (a) flanked by two dsDNA handles (29bp each) is tethered between two micron-sized beads. In the experiments the trap is moved relative to the pipette at speeds ranging from 10 to 1000nm/s. (c) Different force cycles recorded at 300nm/s. The red curves indicate the stretching parts of the cycle whereas the orange curves indicate the releasing parts of the cycle. Note that the forces of unfolding and refolding are random due to the stochastic nature of the thermally activated unfolding/folding process. The marked hysteresis is a signature of an irreversible process. (d) Measurement of work for a single trajectory. It is given by the area below the force-distance curve integrated between two trap positions. Trap distances are relative. Note that there might be more than one unfolding or refolding event along each trajectory. $f^*(S)(f^*(R))$ defines the first rupture force in the unfolding (refolding) process. Figure taken from [30].

apply the time-reversed protocol for $\lambda(t)$ and the DNA hairpin recovers its native conformation. When unzipping short hairpins, a jump in force is generally observed in the force-distance curve (FDC), characteristic of two-states systems: either the hairpin is folded or it is unfolded (see Fig. 1d). In contrast, large hairpins tend to display different levels of rupture force corresponding to different intermediates. The unraveling of rupture process is thermally activated, and the force at which the hairpin unfolds or refolds changes in each cycle, as shown in Fig. 1c. Depending on the pulling speed, FDCs reveal different degree of hysteresis.

4 Fluctuation relations

Fluctuation relations (FR) establish fundamental equalities between the work applied in non-equilibrium systems and FE differences. As such they overcome some of the limitations of classical FE measurement techniques, introduced in Section 2.

To better understand FR consider a generic system in thermal equilibrium that is transiently driven out of equilibrium during the time interval [0, t_B] by varying λ according to a protocol $\lambda(t)$ (hereafter referred as the forward protocol) from an initial value $\lambda(0) = \lambda_A$ to a final value $\lambda(t_B) = \lambda_B$. The work W measured along the trajectory significantly changes in each realization because it is not possible to control the configurations explored by the system: work fluctuations are of the same order of magnitude than energy exchanges with the environment. According to the second law of thermodynamics, the average of the work over multiple independent realizations of the experiment is larger than or equal (if the perturbation is slow enough) to the FE difference between the initial and the final states, $\langle W \rangle = W_{rev} + \langle W \rangle_{dis} \geq \Delta G$. Thus, the faster the perturbation, the larger the dissipated work $\langle W \rangle_{dis}$. Let us consider also the reversed process where the system starts in equilibrium at λ_B and λ is varied according to the time reversal protocol, $\lambda(t_B - t)$, until reaching the final value λ_A (see Fig. 2).

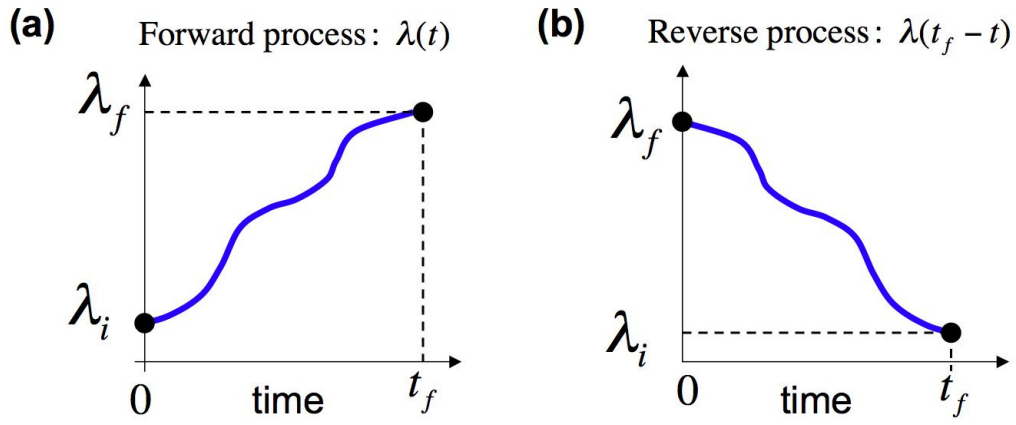

Figure 2: **Forward and reverse paths.** (a) An arbitrary forward protocol. The system starts in equilibrium at λ_A and is transiently driven out of equilibrium until λ_B. At λ_B the system may be or not in equilibrium. (b) The reverse protocol of (a). The system starts in equilibrium at λ_B and is transiently driven out of equilibrium until λ_A. At λ_A the system may be or not in equilibrium.

An important FR is the Crooks fluctuation relation (CFR), that reads as [7, 8]:

$$\frac{P_F(W)}{P_R(-W)} = \exp\left(\frac{W - \Delta G}{k_B T}\right), \tag{9}$$

Where $P_F(W)$ is the probability density function of the work performed along the forward protocol, $P_R(-W)$ is the probability density function of the work performed along the reversed protocol, and $\Delta G = G(\lambda_B) - G(\lambda_A)$ is equal to the Gibbs Free Energy difference between the equilibrium states at λ_B and λ_A. In single molecule experiments pressure and temperature are usually controlled, so that the Gibbs Free Energy is the relevant quantity. An important consequence of Eq. (9) is that the FE difference corresponds to the work equally probable in

both the forward and the reversed protocol, which is always the same no matter how far from equilibrium the system is brought under the perturbative protocol. An equally important result is the prediction of the existence of trajectories where the dissipated work is negative, meaning that heat from the environment is absorbed and converted into useful work. It must be stressed that there is no violation of the second law because thermodynamics does not focus on a single trajectory but on the average over an infinite number of them.

Particular corollaries of the CFR can be obtained by integration of Eq. (9). For instance, if we multiply and divide the l.h.s. of Eq. (9) by a generic function $\phi(W)$ and integrate over W we get:

$$e^{-\frac{\Delta G}{k_{\mathrm{B}}T}} = \frac{\langle e^{-\frac{W}{k_{\mathrm{B}}T}}\phi(W)\rangle_F}{\langle \phi(-W)\rangle_R} \tag{10}$$

where $\langle \dots \rangle_{F(R)}$ denote the average over forward(reversed) trajectories. When $\phi(W) = 1$ we get the well-known Jarzynski equality, $e^{-\Delta G/k_{\mathrm{B}}T} = \langle e^{-W/k_{\mathrm{B}}T}\rangle$ [20], that has been used for FE recovery [19, 24]. However this expression is strongly biased for a finite number of measurements [48, 37]. More information is given in Section 7. Bidirectional methods that combine information from the forward and reverse processes and use the CFR have proven to be more predictive [3, 42, 26].

4.1 Experimental validation of the Crooks equality

The CFR was experimentally tested in 2005 in RNA pulling experiments with laser tweezers [6] showing this to be a reliable and useful methodology to extract FE differences between states that could not be measured with bulk methods. The forward(reversed) process is identified with the unzipping(rezipping) of the hairpin, that starts in $\lambda_A(\lambda_B)$ where the hairpin is folded(unfolded). The work is evaluated as the area below the experimental FDC (see Fig. 1d),

$$W = \int_{\lambda_A}^{\lambda_B} f \mathrm{d}\lambda \tag{11}$$

The definition of work is not straightforward. For more information see Section 5. In Fig. 3a we show the experimental $P_F(W)$ and $P_R(-W)$ obtained in pulling experiments at three different pulling speeds for the hairpin sketched Fig. 1a (results obtained in the Small Biosystems Lab in Barcelona using dual-beam miniaturized optical tweezers [30, 25, 18]). Note that the crossing point of the histograms, equal to the FE difference between the final and the initial states, does not depend on the pulling speed, whereas hysteresis effects (and therefore dissipation) increase.

A first validation of Eq. (9) is shown in Fig. 3b, where the logarithm of the ratio between the probabilities $P_F(W)$ and $P_R(-W)$ is represented versus $W - \Delta G$. Note that data collapses in a single straight line with slope almost equal to 1. Therefore, an estimation of the FE of the system is measured by identifying the value of work at which $\log\left[P_F(W)/P_R(-W)\right] = 0$.

However, a proper estimation of the FE using Eq. (9) is limited by the number of unzipping and rezipping cycles. If we do not have enough data, the tail of the work distributions is not well-captured and a bias is introduced in the FE estimation. Several procedures have been proposed in literature to beat this inconvenience (more information is given in Section 7). Here we present the Bennett acceptance ratio method [3] as a first approach to estimate FE differences. This method consists on using the following function $\phi(W)$ in Eq. (10):

$$\phi(W) = \frac{1}{1 + \frac{n_F}{n_R}\exp\left(\frac{W-\Delta G}{k_{\mathrm{B}}T}\right)} \tag{12}$$

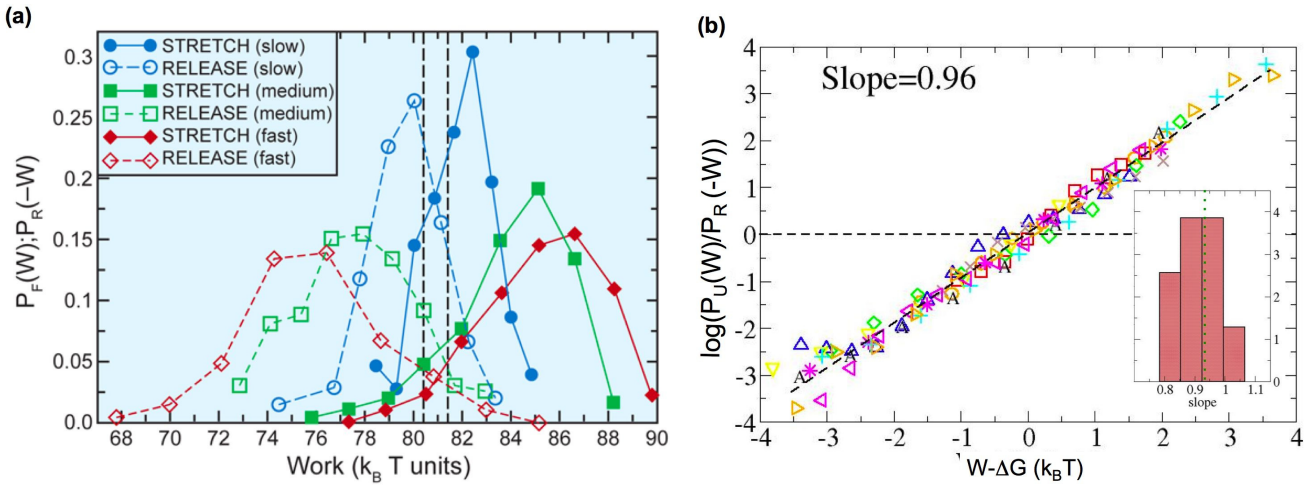

Figure 3: **The Crooks fluctuation relation.**(a) Work distributions for the hairpin shown in Figure 1 measured at three different pulling speeds: 50 nm/s (blue), 100 nm/s (green) and 300 nm/s (red). Unfolding or forward (continuous lines) and refolding or reverse work distributions (dashed lines) cross each other at a a value 81.0±0.2 $k_{\rm B}T$ independent of the pulling speed.(b) Experimental test of the CFR for 10 different molecules pulled at different speeds. The log of the ratio between the unfolding and refolding work distributions is equal to $(W-\Delta G)$ in $k_{\rm B}T$ units. The inset shows the distribution of slopes for the different molecules which are clustered around an average value of 0.96. Figure taken from [30].

where n_F and n_R are the number of measured forward and reversed trajectories. This function is known to minimize the statistical variance of the estimation of the FE difference ΔG. Therefore, we estimate the FE difference as the solution to the transcendental equation:

$$\begin{aligned}\frac{u}{k_{\rm B}T} &= z(u) \\ &= -\log\left\langle \frac{e^{-\frac{W}{k_{\rm B}T}}}{1+\frac{n_F}{n_R}e^{\frac{W-u}{k_{\rm B}T}}}\right\rangle_F + \log\left\langle \frac{1}{1+\frac{n_F}{n_R}e^{-\frac{W+u}{k_{\rm B}T}}}\right\rangle_R \end{aligned} \tag{13}$$

The FE estimate is the FE difference of the total system (hairpin, handles and bead) between the initial and the final states. In order to obtain the FE of formation of the hairpin, we need to subtract the contributions coming from the work performed by the trap to stretch the handles, pull on the bead and stretch the elastic ssDNA released when the hairpin unfolds [30]. Once we do that, we obtain that the FE of the hairpin sketched in Fig. 1 and whose experimental data is shown in Fig. 3 is 61.0±0.5 $k_{\rm B}T$, which is in fair agreement with the predicted FE obtained from calorimetric melting experiments, 60.53 $k_{\rm B}T$ [21, 49].

5 Control parameters, configurational variables and the definition of work

In small systems it is crucial to make a distinction between controlled parameters and non-controlled or fluctuating variables. Controlled parameters are macroscopic variables that are

imposed on the system by the external sources (e.g. the thermal environment) and do not fluctuate with time. In contrast, non-controlled variables are microscopic quantities describing the internal configuration of the system and do fluctuate in time because they are subject to Brownian forces. Let us consider a typical single molecule experiment where a protein is pulled by an AFM. In this case the control parameter is given by the position of the cantilever that determines the degree of stretching and the average tension applied to the ends of the protein. Also the temperature and the pressure inside the fluidic chamber are controlled parameters. However, the height of the tip respect to the substrate or the force acting on the protein are fluctuating variables that describe the molecular extension of the protein tethered between tip and substrate. Also the position of each of the residues along the polypeptide chain are fluctuating variables. Both molecular extension or force and the residues' positions define different types of configurational variables. However only the former are subject to experimental measurement and therefore we will restrict our discussion throughout this paper to such kind of experimentally accessible configurational variables. Fig. 4 illustrates other examples of control parameters and configurational variables. In what follows we will denote by λ the set of controlled (i.e. non-fluctuating) parameters and x the set of configurational (i.e. fluctuating) variables. The definition of what are controlled parameter or configurational variables is broad. For example, a force can be a configurational variable and a molecular extension can be a controlled parameter, or vice versa, depending on the experimental setup (see Fig. 4, right example).

The energy of a system acted by external sources can be generally described by a Hamiltonian or energy function $U(x,\lambda)$. The net variation of U is given by the conservation law,

$$dU = \Big(\frac{\partial U}{\partial x}\Big)dx + \Big(\frac{\partial U}{\partial \lambda}\Big)d\lambda = đQ + đW \tag{14}$$

where $đQ, đW$ stand for the infinitesimal heat and work transferred to the system. The previous mathematical relation has a simple physical interpretation. Heat accounts for the energy transferred to the system when the configurational variables change at fixed value of the control parameter. Work is the energy delivered to the system by the external sources upon changing the control parameter for a given configuration. The total work performed by the sources on the system when the control parameter is varied from λ_A to λ_B is given by,

$$W = \int_{\lambda_A}^{\lambda_B} đW = \int_{\lambda_A}^{\lambda_B} \Big(\frac{\partial U}{\partial \lambda}\Big)d\lambda = \int_{\lambda_A}^{\lambda_B} F(x,\lambda)d\lambda \tag{15}$$

where $F(x,\lambda)$ is a generalized force defined as,

$$F(x,\lambda) = \Big(\frac{\partial U}{\partial \lambda}\Big) \qquad . \tag{16}$$

It is important to stress that the generalized force is not necessarily equal to the mechanical force acting on the system. In other words, $F(x,\lambda)$ is a configurational dependent variable conjugated to the control parameter λ and has dimensions of [energy]/[λ] which are not necessarily Newtons. In the example shown in the right of Fig. 4 the control parameter is the magnetic force $\lambda \equiv f$ and the configurational variable x is the molecular extension of the polymer. The total Hamiltonian of the system is then given by $U(x,f) = U_0(x) - fx$ where $U_0(x)$ is the energy of the system at $\lambda = f = 0$. In other words, the external force f shifts all energy levels (defined by x) of the original system by the amount -fx. The generalized force is then given by $F(x,f) = -x$ (i.e. it has the dimensions of a length) and $đW = -xdf$. The fact that $đW$ is equal to $-xdf$ and not equal to fdx has generated some controversy over the past years [32]. Below we show how this distinction is already important for the simplest case of a bead in the optical trap. In Section 5.1 we also show how the physically sound definition of mechanical work is amenable to experimental test.

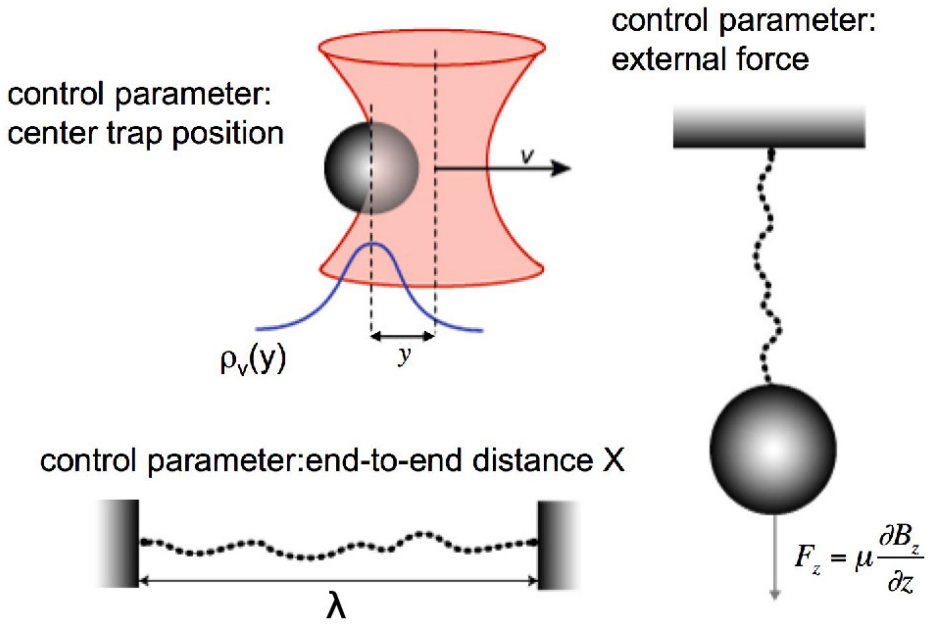

Figure 4: **Control parameter and configurational variables.** Different experimental setups corresponding to different types of control parameters (denoted as λ) or configurational variables (denoted as x). (Top left) A micron-sized bead dragged through water. λ could be the center of the trap measured in the lab (i.e. fixed to the water) frame whereas x is the displacement of the bead, indicated as y, respect to the center of the trap. (Bottom left) A polymer tethered between two surfaces. λ is the distance between the surfaces and x the force acting on the polymer. (Right) A polymer stretched with magnetic tweezers. λ is the force acting on the magnetic bead and x is the molecular extension of the tether.

5.1 About the right definition of work: accumulated versus transferred work

In a pulling experiment with OT (see Section 3.2) there are two possible representations of the pulling curves (Fig. 5b). In one representation the force is plotted versus the relative trap-pipette distance (λ), the so-called force-distance curve (hereafter referred as FDC). In the other representation the force is plotted versus the relative molecular extension (x), the so-called force-extension curve (hereafter referred as FEC). In the optical tweezers setup $\lambda = x + y$ where y is the distance between the bead and the center of the trap. The measured force is given by $F = ky$ where k is the stiffness of the trap. The areas below the FDC and the FEC define two possible work quantities, $W = \int_{\lambda_A}^{\lambda_B} F d\lambda$ and $W' = \int_{x_A}^{x_B} F dx$. If the bead and the molecular system are in mechanical equilibrium then the average forces acting on bead and molecule are identical. From the relation $d\lambda = dx + dy$ we get,

$$W = W' + W_b = W' + \frac{F_B^2 - F_A^2}{2k} \tag{17}$$

where F_A, F_B are the initial and final forces along a given trajectory. W is often called the total accumulated work and contains the work exerted to displace the bead in the trap, W_b, and the work transferred to the molecular system, W' (therefore receiving the name of transferred work) [40, 29]. The term W_b appearing in Eq.(17) implies that W, W' cannot simultaneously satisfy the CFR. What is the right definition of the mechanical work? In other words, which work definition satisfies the CFR? The answer to our question is straightforward if we correctly identify which are the control parameters and which are the configurational variables. In the lab frame defined by the pipette (or by the fluidic chamber to which the pipette is glued) the control parameter λ is given by the relative trap-pipette distance, whereas the molecular extension x stands for the configurational variable. Note that, due to the non-invariance property of the CFR under Galilean transformations, y cannot be used as configurational variable because it is defined respect to the co-moving frame defined by the trap. The total energy of the molecular system is then given by $U(x, \lambda) = U_m(x) + (k/2)(\lambda - x)^2$ where $U_m(x)$ is the energy of the molecular system. From Eq.(16) and using $\lambda = x + y$ we get $F = ky = k(\lambda - x)$. From Eq.(15) we then conclude that the mechanical work that satisfies the CFR is the accumulated work W rather than the transferred work W'. We remark a few relevant facts,

1. **The transferred work W' does not satisfy the CFR and is dependent on the bandwidth of the measurement.** The FDC and FEC are sensitive to the bandwidth or data acquisition rate of the measurement (Fig. 5b). Whereas W is insensitive to the bandwidth W' is not (see Fig. 6a). This difference is very important because it implies that the bandwidth dependence implicit in the boundary term in Eq.(17) (the power spectrum of the force depends on the bandwidth if this is much smaller than the corner frequency of the bead) is fully contained in W'. Operationally it is much easier to use W rather than W'. As shown in Fig. 6b, W satisfies the CFR whereas W' does not. The logarithm of the ratio $\log(P_F(W')/P_R(-W'))$ plotted versus W'/k_BT is strongly bandwidth dependent and exhibits a slope 30 times smaller than 1 (i.e. the slope expected for W from the CFR) [29].

2. **How big is the error made in recovering free energy differences by using W' rather than W?** Despite that W and W' only differ by a boundary term (cf. Eq.17) one can show that, for the case of the mechanical folding/unfolding of the hairpin, the error in recovering FE differences using the Jarzynski equality can be as large as 100% [29]. The error or discrepancy increases with the bandwidth. Interestingly enough, for small enough

bandwidths (but always larger than the coexistence kinetic rates between the folded and unfolded states, otherwise the folding/unfolding transitions are smeared out) fluctuations in the boundary term in Eq.(17) are negligible and both W and W' are equally good. This explains why previous experimental tests of the CFR that used W' instead of W produced satisfactory results (e.g. [6]).

3. **Nonequivalence between moving the trap and the pipette or chamber.** The non-invariance of the CFR under Galilean transformations suggests that moving the optical trap inside the fluidic chamber should not be necessarily equivalent to moving the pipette glued to the fluidic chamber. We have to distinguish two cases depending on whether the fluid inside the chamber is dragged (*stick* conditions) or not (*slip* conditions) by the moving chamber. The two scenarios are physically different because in the former case the bead in the trap is subject to an additional Stokes force due to the motion of the fluid. If the fluid is not dragged by the moving chamber (*slip* conditions) then y is the right configurational variable. In this case, $U(y,\lambda) = U_m(\lambda - y) + (k/2)(y)^2$ and the generalized force is equal to $F = U'_m(\lambda - y)$. Note that this F is not equal to the instantaneous force measured by the optical trap but the instantaneous force acting on the molecule. Even in case of mechanical equilibrium the difference between the two instantaneous forces, $U'_m(\lambda - y)$ and ky, produces a net non-negligible difference term. If the fluid does move with the chamber (*stick* conditions) then y is again the right configurational variable and we recover the main results of this section. Interestingly, all experiments done until now that use motorized stages to move chambers operate in *stick* conditions so we do not expect experimental discrepancies for the definition of the work.

4. **Other cases where the work definition matters.** As we showed in Fig. 6 the CFR and the right definition of work W are both amenable to experimental test. Another interesting example where the boundary term is relevant is when the force f (rather than the trap position) is controlled. As we saw in Section 5 the work in that case is given by $W_{X_0} = -\int_{f_A}^{f_B} X df$ where $X = y + x + X_0$ is the absolute trap-pipette distance. Because X_0 stands for an arbitrary origin, the work W_{X_0} is also a quantity that depends on X_0. This may seem unphysical but it is not [32]. The CFR is invariant respect to the value of X_0 as it can be easily checked by writing, $W_{X_0} = W_{X_0=0} - X_0(f_B - f_A)$, and using Eq.(9) gives $\Delta G_{X_0} = \Delta G_{X_0=0} - f X_0$. If the force f is controlled, then other work related quantities such as $W' = \int_{x_A}^{x_B} f dx$ or $W'' = \int_{X_A}^{X_B} f dX$ differ from W by finite boundary terms. Again these terms make the CFR not to be satisfied for W' and W''. These predictions are amenable to experimental test in magnetic tweezers (where the force is naturally controlled) or in optical tweezers operating in the force clamp mode with infinite bandwidth [13], or even in a force feedback mode with finite bandwidth as well.

6 Extended fluctuation relations

The growing theoretical understanding of Fluctuation Theorems has led to the development of different tools, especially suited to measure FE differences under special requirements. For example the CFR can be generalized to cases where the system is initially in partial, rather than global, equilibrium both in the forward and the reverse protocol [22]. Suppose we take a system at fixed control parameter λ in thermal equilibrium with a bath at temperature T. The probability distribution over configurational variables x is Gibbsian over the whole phase space S meaning that: $P^{\rm eq}_\lambda(x) = \exp(-E_\lambda(x)/k_{\rm B}T)/Z_\lambda$ with Z_λ the partition function $Z_\lambda =$

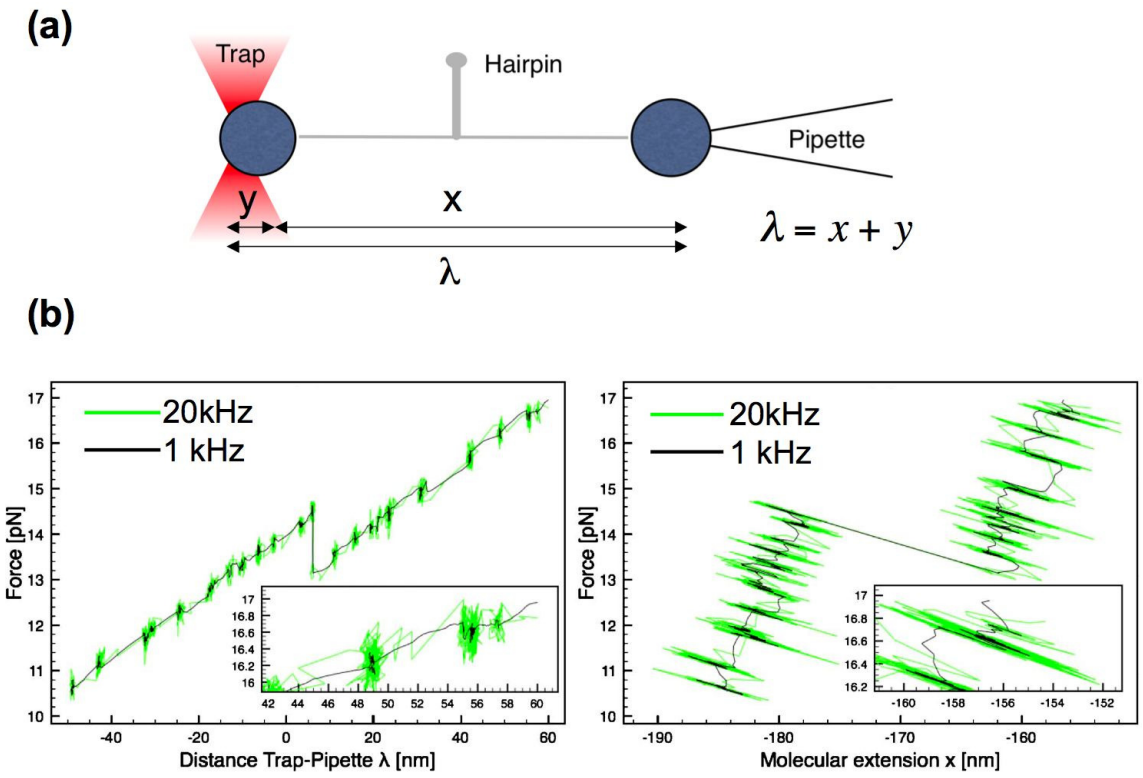

Figure 5: **FDC versus FEC.** (a) Experimental setup and different variables. (b) The FDC and FEC are defined as the curves obtained by plotting the force versus the trap position or the molecular extension respectively. Although force fluctuations in both types of curves show a dependence with the bandwidth of the measurement (black, 1kHz; green 20 kHz) only in the FEC the measurement of the work is very sensitive to such fluctuations. Figure taken from [29]

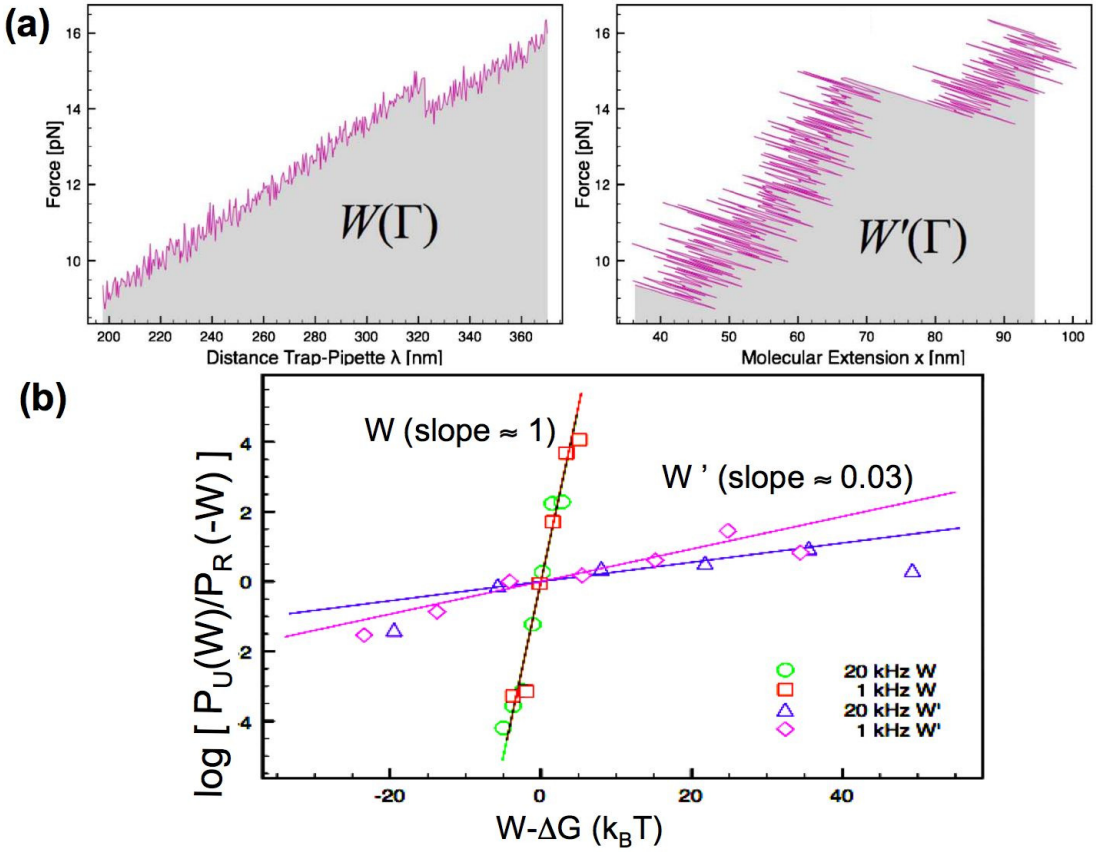

Figure 6: **Accumulated (W) versus transferred (W') work.** (a) The two work quantities for a given experimental trajectory. Note that the effect of bandwidth dependent force fluctuations is much larger for W' as compared to W, showing the importance of the boundary term Eq.17. (b) Experimental test of the CFR. When using W the CFR is satisfied at all bandwidths. However when we use W' the CFR is strongly violated and dependent on the measurement bandwidth. Figure taken from [29]

$\sum_{x\in S}\exp(-E_\lambda(x)/k_{\rm B}T)$, where $E_\lambda(x)$ is the energy function of the system for a given pair λ, x. We refer to this condition as global thermodynamic equilibrium. However we might consider a case where the initial state is Gibbsian but restricted over a subset of configurations $S'\subseteq S$. We refer to this case as partial thermodynamic equilibrium. Partially equilibrated states satisfy $P^{\rm eq}_{\lambda,S'}(x)=P^{\rm eq}_{\lambda}(x)\chi_{S'}(x)Z_\lambda/Z_{\lambda,S'}$, where $\chi_{S'}$ is the characteristic function defined over the subset $S'\subseteq S$ ($\chi_{S'}=1$ if $x\in S'$ and zero otherwise), and $Z_{\lambda,S'}$ is the partition function restricted to the subset S', i.e. $Z_{\lambda,S'}=\sum_{x\in S'}\exp(-E_\lambda(x)/k_{\rm B}T)$. The partial FE is then given by $G_{\lambda,S'}=-k_{\rm B}T\log Z_{\lambda,S'}$. Let us suppose the following scenario: along the forward process the system is initially in partial equilibrium in S_A at λ_A, and along the reverse process the system is initially in partial equilibrium in S_B at λ_B. The extended CFR reads,

$$\frac{p_{\rm F}^{S_A\to S_B}}{p_{\rm R}^{S_A\leftarrow S_B}}\frac{P^{S_A\to S_B}(W)}{P^{S_A\leftarrow S_B}(-W)}=\exp[\beta(W-\Delta G^{S_B,\lambda_B}_{S_A,\lambda_A})]\,, \tag{18}$$

where the direction of the arrow distinguishes forward from reverse, $p_{\rm F}^{S_A\to S_B}$ ($p_{\rm R}^{S_A\leftarrow S_B}$) stands for the probability to be in S_B (S_A) at the end of the forward (reverse) process, and $\Delta G^{S_B,\lambda_B}_{S_A,\lambda_A}=G_{S_B}(\lambda_B)-G_{S_A}(\lambda_A)$ is the FE difference between the partially equilibrated states S_A and S_B. Partially equilibrated states appear in many cases, from protein and peptide-nucleic acid binding to intermediate and misfolded molecular states.

The usefulness of the extended CFR relies on our possibility to experimentally distinguish the different kinetic states along any trajectory. For example, a molecule pulled by stretching forces can be in partial equilibrium when it stays either in the folded or unfolded state until it transits to the other state. If S_A stands for the folded state and S_B for the unfolded state, the extended CFR makes possible to extract the free energies $G_{S'}(\lambda)$ of the folded and unfolded states $S'=S_A$, S_B along the λ-axis, i.e. the folded and unfolded branches. Fig. 7 shows an experimental verification of this result for a two-states molecule.

It is worth mentioning that Eq. (18) leads to a extended Jarzynski equality for kinetic states,

$$\left\langle\exp\left(-\frac{W-\Delta G^{S_B,\lambda_B}_{S_A,\lambda_A}}{k_{\rm B}T}\right)\right\rangle=\frac{p_{\rm R}^{S_A\leftarrow S_B}}{p_{\rm F}^{S_A\to S_B}} \tag{19}$$

This expression is formally equivalent to a recently proposed generalization of the Jarzynski equality to systems with a feedback control [38, 43]:

$$\left\langle\exp\left(-\frac{W-\Delta G^{S_B,\lambda_B}_{S_A,\lambda_A}}{k_{\rm B}T}\right)\right\rangle=\gamma \tag{20}$$

where γ quantifies how efficiently the obtained information is used for the feedback control. Note that both equations use more information about the response of the system during the perturbative protocol than just the total work. In Eq. (19) the trajectories are classified according to the initial and final state to measure free energy differences, an operation which can be carried out *a posteriori*. In contrast in Eq. (20) the response of the system influences the protocol itself in a feedback loop. The formal similarity of these two equations leaves the open question of whether the operation of classifying trajectories can be considered as a feedback.

6.1 Experimental measurement of the potential of mean force

Another interesting physical quantity is the so-called *potential of mean force*, which is the Free Energy as a function of a reaction coordinate. This specific case was considered by Hummer

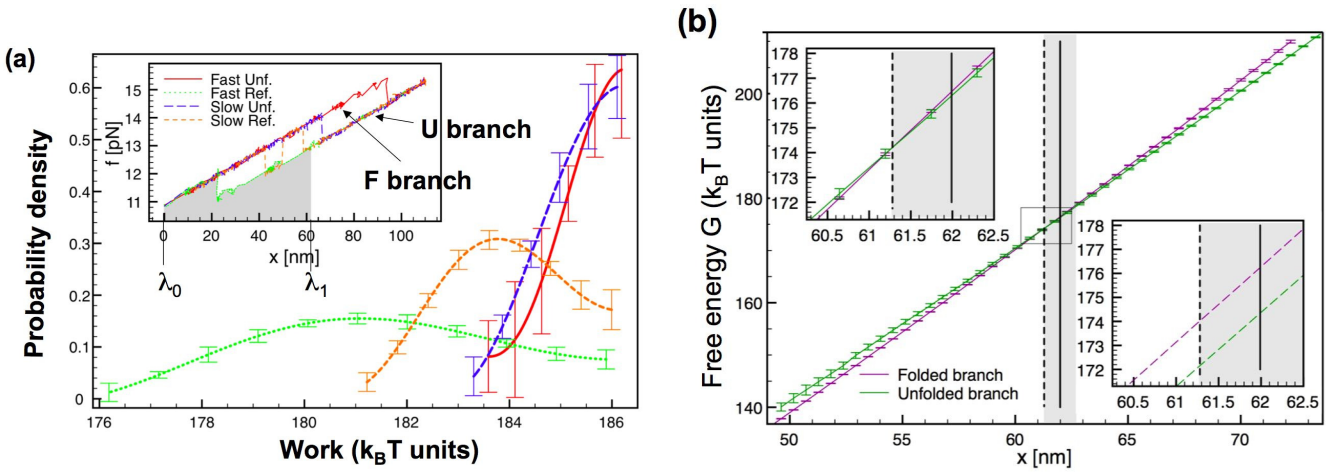

Figure 7: **The extended Crooks fluctuation relation.** (a) Constrained work distributions measured in a 20bp hairpin at two different pulling speeds: 300nm/s (red, unfolding; green, refolding) and 40nm/s (blue, unfolding; orange, refolding). (a,Inset) The forward trajectories we consider are those where the hairpin starts partially equilibrated in the folded (F) state at λ_A and ends in the unfolded (U) state (partially equilibrated or not) at λ_B.Note that, due to the correction term $p_{\rm F}^{F\to U}/p_{\rm R}^{F\leftarrow U}$ appearing in Eq.(18), restricted unfolding and refolding work distributions should not cross each other at an energy value that is independent of the pulling speed. (b) Reconstruction of the folded (cyan color) and unfolded (green) free energy branches by applying the extended CFR Eq.(18) as shown in (a) and by varying the parameter $x \equiv \lambda_B$. The two branches cross each other around $x_c \simeq 62nm$ corresponding to the coexistence transition. For $x < x_c$ ($x > x_c$) the F (U) state is the minimum free energy state. The upper left inset shows an enlarged view of the crossing region. The lower left region shows the importance of the correction term $p_{\rm F}^{F\to U}/p_{\rm R}^{F\leftarrow U}$ appearing in Eq.(18). If that term was not included in Eq.(18) the coexistence transition disappears. Figure taken from [22]

and Szabo [19], with regard to unidirectional measurements, using the molecular extension as reaction coordinate in pulling experiments:

$$G(x) = -k_{\mathrm{B}}T \log \left\langle \delta(x - x_t) \exp\left(-\frac{W}{k_{\mathrm{B}}T}\right) \right\rangle. \tag{21}$$

Here x_t is the molecular extension at the end of the pulling process and $G(x)$ is the total Free Energy at fixed molecular extension. The Free Energy Surface (FES) of the molecule can then be obtained by subtracting the contributions due to beads and handles from $G(x)$. The theory was later extended by Minh and Adib [26] to take into account bidirectional measurements. These methods have been applied to study the FES of proteins domains [15] and of DNA hairpins [14].

The recovery of FESs or Free Energy Branches (Fig. 7b) can be seen as two different applications of extended fluctuation relations. In the first case, Eq. (18), the method provides the FE of a system partially equilibrated at a given molecular extension, while in the second case, Eq. (21), the system is partially equilibrated in a given state. Indeed Eq. (18) can be cast in a form very similar to Eq. (21). Imagine to study a molecule whose initial state is definite ($S_A = A$) but which can be in different states at the end of the forward protocol ($S_B \in \{B_1, B_2, \dots\}$). In this case, according to the notation of the previous section we have:

$$p_{\mathrm{F}}^{S_A \to S_B} = \langle \delta\left(S_B = B\right) \rangle \tag{22}$$

$$p_{\mathrm{R}}^{S_A \leftarrow S_B} = 1. \tag{23}$$

Now, we introduce Eqs. (22) and (23) inside Eq. (18) and, after rearranging the different terms and integrating both sides over work values we get:

$$\left\langle \exp\left(-\frac{W}{k_{\mathrm{B}}T}\right) \right\rangle^{A \to B} \langle \delta\left(S_B = B\right) \rangle = \exp\left(-\frac{\Delta G_{A,\lambda_A}^{B,\lambda_B}}{k_{\mathrm{B}}T}\right). \tag{24}$$

To cast this last equation in the form of Eq. (21) we need to transform the restricted average over trajectories going from A to B to an average over all trajectories. This can be done using the following identity:

$$\langle \mathcal{O} \rangle^{A \to B} = \frac{\langle \mathcal{O} \delta\left(S_B = B\right) \rangle}{\langle \delta\left(S_B = B\right) \rangle}, \tag{25}$$

where $\langle \dots \rangle$ is the unrestriced average over all trajectories and $\mathcal{O}$ respresents any observable of the system. Finally:

$$\Delta G_{A,\lambda_A}^{B,\lambda_B} = -k_{\mathrm{B}}T \log \left\langle \exp\left(-\frac{W}{k_{\mathrm{B}}T}\right) \delta\left(S_B = B\right) \right\rangle. \tag{26}$$

If now the final condition is a given molecular extension, the method by Hummer and Szabo, Eq. (21), is recovered. Otherwise if the final condition is a given state (native, intermediate, misfolded), we fall back to the case discussed in the previous section.

7 Free energy recovery from unidirectional work measurements

Free energy recovery from irreversible pulling experiments might be done by applying the Jarzynski equality or the Crooks fluctuation relation to unidirectional or bidirectional work measurements respectively. By combining information from the forward and reverse processes, bidirectional methods provide less biased free energy estimates than unidirectional methods. However

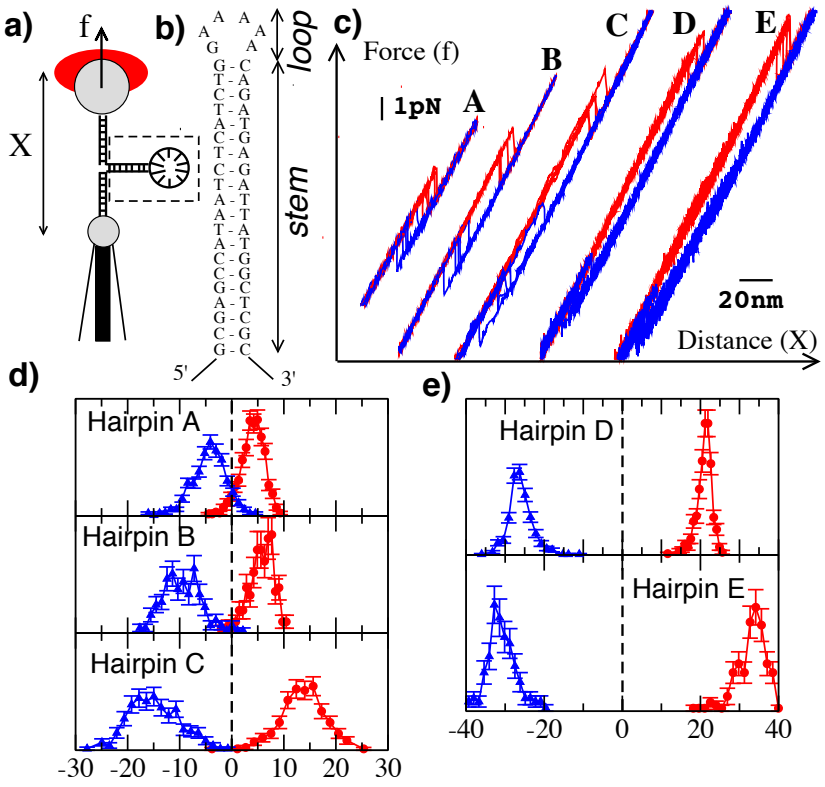

Figure 8: **Work distributions in DNA hairpins of varying loop size.** a) Experimental setup. The DNA hairpin (squared region) is linked to the two microspheres by short (29bp) dsDNA handles [9]. b) Hairpin sequences. The stem is fixed and the size of the loop (sequence 5'-GAAA..-3') takes the values 4,6,12,16,20 (hairpins A,B,C,D,E respectively). c) FDC for the different DNA hairpin sequences. For each sequence different unfolding (red curves) and folding (blue curves) cycles are shown. As the loop size increases FDC tend exhibit larger hysteresis indicating a more irreversible unfolding/folding process. d) and e) Work distributions measured for all sequences (red, unfolding; blue, folding). In the horizontal axis the dissipated work, $W - \Delta G$, is shown in $k_B T$ units with ΔG estimated from combining unidirectional and bidirectional estimates [31]. For hairpins A,B,C a crossing at $W - \Delta G = 0$ is apparent whereas for hairpins D,E it must be guessed. In the latter strongly dissipative regime it is very difficult to extract the value of ΔG from unidirectional work measurements, unless the mathematical form of the work tails spanning the whole range of unfolding and folding work values is known. Panels a),b),c) are taken from [31].

in many situations dissipation is high and the bias obtained by applying any of the two methods is so large that a theory for the bias is needed to reduce the uncertainty. Highly irreversible conditions are found in mechanically unfolding molecular objects that exhibit low thermodynamic stability but high kinetic stability. In this case a large hysteresis is observed between the forward and reverse force-distance curves in pulling cycles. Consequently, the forward and reverse work distributions tend to appear separated by a large gap of empty events along the work axis and the error in predicting free energy differences appears too large using any standard statistical methods. Examples of highly dissipative systems are found in many proteins that are stabilized in their native state by intramolecular contacts that often display a large kinetic stability. Other cases include RNA or DNA molecules stabilized by ligands, or cases in which the experimental technique makes it difficult to see the reverse process e.g. stretching polyproteins with AFM [15]. In general, any molecular complex exhibiting free energy landscapes with a high energy activation state along the reaction pathway (e.g. during unfolding) will tend to exhibit large differences between work values measured along the forward and reverse protocols. In these conditions it might be useful to improve free energy predictions from unidirectional work measurements using theory-based methods that predict how the free energy estimator depends on the number of experiments (N). Despite the large amount of works along this direction only a few analytical results are available. Recently it was shown how it is possible to apply disordered systems theory based on the Random Energy model to predict the dependence of the bias of the Jarzynski estimator on the number of work measurements [31]. By assuming a generalized compressed exponential work distribution with unbounded lower tail it has been possible to extract formulae for the N-dependence of the Jarzynski free energy estimator that match reasonably well the experimental results obtained in DNA hairpins with varying loop sizes (Figure 8). The main drawback of this methodology is the assumption of a specific form for the unbounded tail of the work distribution. Beyond the measurement of few hundreds or thousands of work values, accurate information about the mathematical form of the unbounded tail of the work distribution is generally missing. Indeed exact analytical results obtained in two-level systems [34] and molecular dynamics simulations of mechanical unfolding of peptides [33] show that the unbounded left tail of work distributions are rather described by functions more complex than just compressed exponentials. These distributions have tails interpolating between Gaussian fluctuations around the most probable work and an exponential decay further out in the tail. A thorough analysis of the Jarzynski estimator in strongly dissipative systems should make assumptions about the shape of work tails, possibly obtained from exactly solvable models. Otherwise the error committed in estimating free energy differences from unidirectional work measurements can be too large.

8 Conclusions

The use of fluctuation relations for free energy recovery in single molecule experiments is now a well-established methodology. Future perspectives in this field aim to extend the applicability of this techniques from the now classical example of two-states DNA hairpins to more complex situations. For instance, the technique described in Section 6 can be applied to study the thermodynamics of intermediates and misfolded states. Such kinetic states, which are hardly observed in classical experiments (Section 2), are crucial, for example, to understand the folding behavior of proteins. Moreover, the same method could be applied to study the energetics of binding of proteins or drugs to nucleic acids.

The applicability of fluctuations relations is limited in systems with large dissipation, where free energy estimations can be strongly biased. This is the case, for instance, of many proteins under pulling experiments [41]. A boost in the investigation of protein stability by single

molecule manipulation and nonequilibrium experiments could be provided by the improvement and application of the technique discussed in Section 7.

Finally, the recent results in thermodynamics of feedback protocols [38, 43, 16] have not found their application to single molecule experiments yet. For instance, they could be useful in designing new experimental protocols to reduce the bias and improve free energy estimates.

Overall, the application of fluctuation theorems to free energy recovery is a rapidly evolving field, both from the theoretical and experimental perspectives. Many exciting developments are to be expected.

References

[1] A. Alemany, M. Ribezzi, and F. Ritort. Recent progress in fluctuation theorems and free energy recovery. In *Non-equilibrium statistical physics today*, 2011.

[2] P. Atkins and J. de Paula. Elements of physical chemistry, 2009.

[3] C.H. Bennett. Efficient estimation of free energy differences from monte carlo data. *Journal of Computational Physics*, 22(2):245–268, 1976.

[4] C. Bustamante, J. Liphard, and F. Ritort. The nonequilibrium thermodynamics of small systems. *Physics Today*, 58:43–38, 2005.

[5] C. Chipot and A. Pohorille. *Free energy calculations: theory and applications in chemistry and biology*, volume 86. Springer Verlag, 2007.

[6] D. Collin, F. Ritort, C. Jarzynski, SB Smith, I. Tinoco, and C. Bustamante. Verification of the crooks fluctuation theorem and recovery of rna folding free energies. *Nature*, 437(7056):231–234, 2005.

[7] G. E. Crooks. Entropy production fluctuation theorem and the nonequilibrium work relation for free energy differences. *Phys. Rev. E*, 60:2721, 1999.

[8] G. E. Crooks. Path-ensemble averages in systems driven far from equilibrium. *Phys. Rev. E*, 61:2361–2366, 2000.

[9] N. Forns, S. de Lorenzo, S. Manosas, K. Hayashi, J. M. Huguet, and F. Ritort. Single-molecule experiments using molecular constructs with short handles. *Biophysical Journal*, 100:1765–1774, 2011.

[10] A. Galera-Prat, A. Gómez-Sicilia, A. F. Oberhauser, M. Cieplak, and M. Carrión-Vázquez. Understanding biology by stretching proteins: recent progress. *Curr. Opin. Struct. Biol.*, 20 (1):63–9, 2010.

[11] C. Gossel and V. Croquette. Magnetic tweezers: Micromanipulation and force measurement at the molecular level. *Biophysical Journal*, 82 (6):3314–3329, 2002.

[12] N.J. Greenfield. Using circular dichroism spectra to estimate protein secondary structure. *Nature protocols*, 1(6):2876, 2006.

[13] J. W. Greenleaf, M. T. Woodside, E. A. Abbondanzieri, and S. M. Block. Passive all-optical force clamp for high-resolution laser trapping. *Physical Review Letters*, 95:218102, 2005.

[14] A. N. Grupta, A. Vincent, K. Neupane, H. Yu, F. Wang, and M. T. Woodside. Experimental validation of free-energy-landscape reconstruction from non-equilibrium single-molecule force spectroscopy measurements. *Nature Physics*, 7:631–634, 2011.

[15] N.C. Harris, Y. Song, and C.H. Kiang. Experimental free energy surface reconstruction from single-molecule force spectroscopy using jarzynskis equality. *Physical review letters*, 99(6):68101, 2007.

[16] Jordan M. Horowitz and Suriyanarayanan Vaikuntanathan. Nonequilibrium detailed fluctuation theorem for repeated discrete feedback. *Phys. Rev. E*, 82:061120, 2010.

[17] T. Hugel and M. Seitz. The study of molecular interactions by afm force spectroscopy. *Macromolecular rapid communications*, 22 (13):989–1016, 2001.

[18] J. M. Huguet, C. V. Bizarro, N. Forns, S. B. Smith, C. Bustamante, and F. Ritort. Single-molecule derivation of salt dependent base-pair free. *Proceedings of the National Academy of Sciences*, 107:15431–15436, 2010.

[19] G. Hummer and A. Szabo. Free energy reconstruction from nonequilibrium single-molecule pulling experiments. *Proceedings of the National Academy of Sciences*, 98(7):3658, 2001.

[20] C. Jarzynski. Nonequilibrium equality for free energy differences. *Physical Review Letters*, 78(14):2690, 1997.

[21] J. Santalucia Jr. A unified view of polymer, dumbbell, and oligonucleotide dna nearest-neighbor thermodynamics. *Proceedings of the National Academy of Sciences*, 95:1460–1465, 1998.

[22] I. Junier, A. Mossa, M. Manosas, and F. Ritort. Recovery of free energy branches in single molecule experiments. *Physical Review Letters*, 102:070602, 2009.

[23] J.G. Kirkwood. Statistical mechanics of fluid mixtures. *The Journal of Chemical Physics*, 3:300, 1935.

[24] J. Liphardt, S. Dumont, S.B. Smith, I. Tinoco, and C. Bustamante. Equilibrium information from nonequilibrium measurements in an experimental test of jarzynski's equality. *Science*, 296(5574):1832, 2002.

[25] M. Manosas, A. Mossa, N. Forns, J. M. Huguet, and F. Ritort. Dynamic force spectroscopy of dna hairpins (ii): Irreversibility and dissipation. *Journal of Statistical Mechanics: Theory and Experiment*, P02061, 2009.

[26] D.D.L. Minh and A.B. Adib. Optimized free energies from bidirectional single-molecule force spectroscopy. *Physical review letters*, 100(18):180602, 2008.

[27] J.R. Moffitt, Y.R. Chemla, S.B. Smith, and C. Bustamante. Recent advances in optical tweezers. *Annu. Rev. Biochem.*, 77:205–228, 2008.

[28] F. Mosconi, J. F. Allemand, D. Bensimon, and V. Croquette. Measurement of the torque on a single stretched and twisted dna using magnetic tweezers. *Phys. Rev. Lett.*, 201:078301, 2009.

[29] A. Mossa, S. de Lorenzo, J. M. Huguet, and F. Ritort. Measurement of work in single molecule experiments. *Journal of Chemical Physics*, 130:234116, 2009.

[30] A. Mossa, M. Manosas, N. Forns, J. M. Huguet, and F. Ritort. Dynamic force spectroscopy of dna hairpins: I. force kinetics and free energy landscapes. *Journal of Statistical Mechanics: Theory and Experiment*, P02060, 2009.

[31] M. Palassini and F. Ritort. Improving free-energy estimates from unidirectional work measurements: theory and experiment. *Physical Review Letters*, 107:060601, 2011.

[32] L. Peliti. On the work–hamiltonian connection in manipulated systems. *Journal of Statistical Mechanics*, P05002, 2008.

[33] P. Procacci and S. Marsili. Energy dissipation assymetry in the non equilibrium folding/unfolding of the single molecule alanine decapeptide. *Chemical Physics*, 375:8–15, 2010.

[34] F. Ritort. Work and heat fluctuations in two-state systems. *Journal of Statistical Mechanics: Theory and Experiment*, P10016, 2004.

[35] F. Ritort. Single-molecule experiments in biological physics: methods and applications. *Journal of Physics: Condensed Matter*, 18:R531, 2006.

[36] F. Ritort. Nonequilibrium fluctuations in small systems: from physics to biology. *Advances in Chemical Physics*, 137:31–123, 2008.

[37] F. Ritort, C. Bustamante, and I. Tinoco. A two-state kinetic model for the unfolding of single molecules by mechanical force. *Proceedings of the National Academy of Sciences*, 99(21):13544, 2002.

[38] T. Sagawa and M. Ueda. Generalized jarzynski equality under nonequilibrium feedback control. *Physical Review Letters*, 204:2010, 090602.

[39] J.M. Sánchez-Ruiz. Probing free-energy surfaces with differential scanning calorimetry. *Annual Review of Physical Chemistry*, 62 (1), 2011.

[40] J. M. Schurr and S. B. Fujimoto. Equalities for the nonequilibrium work transferred from an external potential to a molecular system. analysis of single-molecule extension experiments. *Journal of Physical Chemistry B*, 107:14007, 2003.

[41] E. A. Shank, C. Cecconi, J. W. Dill, S. Marqusee, and C. Bustamante. The folding cooperative of a protein is controlled by its chain topology. *Nature*, 465:634, 2010.

[42] M.R. Shirts, E. Bair, G. Hooker, and V.S. Pande. Equilibrium free energies from nonequilibrium measurements using maximum-likelihood methods. *Physical review letters*, 91(14):140601, 2003.

[43] S. Toyabe, T. Sagawa, M. Ueda, E. Muneyuki, and M. Sano. Experimental demonstration of information-to-energy conversion and validation of the generalizd jarzynski equality. *Nature Physics*, 6:988–992, 2010.

[44] M.T. Woodside, W.M. Behnke-Parks, K. Larizadeh, K. Travers, D. Herschlag, and S.M. Block. Nanomechanical measurements of the sequence-dependent folding landscapes of single nucleic acid hairpins. *PNAS*, 103(16):6190–6195, 2006.

[45] Min Yao and D. W. Bolen. How valid are denaturant-induced unfolding free energy measurements? level of conformance to common assumptions over an extended range of ribonuclease a stability. *Biochemistry*, 34 (11):3771–3781, 1995.

[46] J. Zlatanova and S. H. Leuba. Magnetic tweezers: a sensitive tool to study dna and chromatin at the single-molecule level. *Biochemistry and Cell Biology*, 81 (3):151–159, 2003.

[47] J. Zlatanova, S. M. Lindscay, and S. H. Leuba. Single molecule force spectroscopy in biology using the atomic force microscope. *Progress in Biophysics and Molecular Biology*, 74:37–61, 2008.

[48] D.M. Zuckerman and T.B. Woolf. Overcoming finite-sampling errors in fast-switching free-energy estimates: extrapolative analysis of a molecular system. *Chemical physics letters*, 351(5-6):445–453, 2002.

[49] M. Zuker. Mfold web server for nucleic acid folding and hybridization prediction. *Nucleic Acids Res.*, 31:3406–3415, 2003.

[50] R.W. Zwanzig. High-temperature equation of state by a perturbation method. i. nonpolar gases. *The Journal of Chemical Physics*, 22:1420, 1954.